Phototransformation pathways of the fungicide dimethomorph((E,Z) 4-[3-(4-chlorophenyl)-(3,4-dimethoxyphenyl)-1-oxo-2-propenyl]morpholine), relevant to sunlit surface waters

Phototransformation pathways of the fungicide dimethomorph ((E,Z) 4-[3-(4-chlorophenyl)-3-(3,4-dimethoxyphenyl)-1-oxo-2-propenyl]morpholine), relevant to sunlit surface waters

Paola Avetta,[a] Giulia Marchetti,[a,b] Marco Minella,[a] Marco Pazzi,[a] Elisa De Laurentiis,[a] Valter Maurino,[a] Claudio Minero,[a] Davide Vione [a,c]*

[a] *Università degli Studi di Torino, Dipartimento di Chimica, Via P. Giuria 5, 10125 Torino, Italy. http://www.chimicadellambiente.unito.it*

[b] *LAV s.r.l., Strada Carignano 58/14, 10024 Moncalieri (TO), Italy. http://www.lavsrl.it*

[c] *Università degli Studi di Torino, Centro Interdipartimentale NatRisk, Via Leonardo da Vinci 44, 10095 Grugliasco (TO), Italy. http://www.natrisk.org*

* Corresponding author. Tel. +39-011-6705296. Fax +39-011-6705242. *davide.vione@unito.it*

Abstract

Dimethomorph (DMM) is a widely used fungicide that shows low toxicity for birds and mammals but can be quite toxic to aquatic organisms. The persistence of DMM in surface waters is thus of high importance, and this work modelled its water half-life time due to photochemical processes. Depending on environmental conditions (*e.g.* water chemistry, depth, season), DMM lifetime could vary from a few days to a few months. For lifetimes of a few weeks or less, photochemistry would be an important pathway for DMM attenuation in surface waters. Such conditions could be reached in summer, in shallow water bodies with low dissolved organic carbon (DOC) and high nitrate and/or nitrite. The main pathways accounting for DMM photodegradation in environmental waters would be the reactions with $^{\bullet}OH$ and with the triplet states of chromophoric dissolved organic matter, $^{3}CDOM^{*}$ (under the hypothesis that $^{3}CDOM^{*}$ reactivity is well described by the triplet state of anthraquinone-2-sulphonate), while direct photolysis would be less important. The $^{\bullet}OH$ pathway would be favoured in low-DOC waters, while the opposite conditions would favour $^{3}CDOM^{*}$. It was possible to detect and identify some intermediates formed upon reaction between DMM and $^{3}CDOM^{*}$, namely N-formylmorpholine, 4-chloroacetophenone and 4-chlorobenzoic acid. The transformation of DMM into the detected compounds would not increase the acute toxicity of the fungicide towards mammals, and the acute effects for freshwater organisms could be decreased significantly.

Keywords: dimethomorph; photochemical transformation; indirect photolysis; environmental persistence of fungicides; agrochemicals.

1. Introduction

The mixture of isomers, (E,Z) 4-[3-(4-chlorophenyl)-3-(3,4-dimethoxyphenyl)-1-oxo-2-propenyl]morpholine (dimethomorph, hereafter DMM) is a systemic morpholine fungicide that is used on several crops including potatoes, tomatoes, grapes, tobacco and tea. To this purpose, it is employed as such or in combined formulations with other fungicides such as mancozeb (manganese ethylenebis(dithiocarbamate) (polymeric) complex with zinc salt) (Stein et al., 2003) or triazole fungicides (*e.g.* hexaconazole) (Baby et. Al., 2004). DMM is an inhibitor of sterol (ergosterol) synthesis and it can be used for the prevention and cure of downy mildews, late blights, crown and root rots (Liu et al., 2012). The effectiveness of DMM as a fungicide was reported for the first time in 1988 (Albert et al., 1988), while its good activity as protectant, curative and antisporulant, especially against downy mildew, was demonstrated by Wicks and Hall (1990).

Despite its beneficial effects in the agricultural field, DMM shows toxicity for several living organisms including soil and water microflora, of which it can alter important biological functions even at very low concentrations (Oliveira et al., 2013). DMM has low toxicity for birds and mammals, but it is slightly to moderately toxic towards fish and invertebrates. Furthermore, DMM has likely synergistic effects with mancozeb and the mixture is highly toxic to freshwater fish and invertebrates (EPA, 1998; Lunn, 2007).

DMM has been detected in surface and ground waters, wastewater, sludge, soils and agricultural products used as food. The concentration values in environmental waters range from ng L^{-1} levels in rivers, to μg L^{-1} levels in wetlands affected by runoff from cultivated soil during precipitation events (EPA, 1998; Maillard et al., 2011). The environmental concentration levels pose limited risk to drinking water sources, but they could be of concern for susceptible aquatic organisms (EPA, 1998; Lunn, 2007).

The pesticide lifetime has been studied in soil, by monitoring its concentration at 10-cm depth after spraying the soil surface with a DMM formulation. Different half-lives have been observed for the E and the Z isomers (~10 and ~30 days, respectively), which could be due to a combination of water solubility and degradation (Liu et al., 2012). Fast E $\rightarrow$ Z photochemical conversion is a potentially important pathway, and it could take place on the soil surface soon after spraying (EPA, 1998; Lunn, 2007). Moreover, DMM is quite resistant to hydrolysis (Lunn, 2007). The half-life time of DMM in soil due to aerobic biodegradation is of the order of a couple of months (Lunn, 2007).

In the literature it is possible to find works concerning the photodegradation of DMM by means of advanced oxidation processes (Yan et al., 2005; Calza et al., 2008, Rashidi et al., 2013, Rashidi et al., 2014), but to our knowledge specific researches dealing with the fate of DMM in natural surface waters have not been published yet. Interestingly, it seems that the only studies investigating the photodegradation of DMM in aqueous solution are unpublished works commissioned by manufacturing companies (Van Dijk, 1990; Knoch and Holman, 1998; Panek et al., 2001), sometimes under conditions that are poorly representative of the aqueous environment

(*e.g.* pH 5). The results of these works are only available as very brief citations in the secondary literature (Lunn, 2007), with difficult or no access to the original papers. Moreover, only direct photolysis seems to have been investigated, which is of limited significance to DMM photoattenuation in surface waters (as will be shown in this work). The scarce available information accounts for the importance of studying DDM photodegradation under conditions that could be relevant to surface waters, where DMM is expected to have a non-negligible impact (EPA, 1998).

In surface water bodies, solar radiation promotes photochemical processes that can be responsible for the photodegradation of organic pollutants. The photoinduced processes are divided in direct photolysis, when the interaction of sunlight with a compound causes its transformation, and indirect photoreactions. The latter involve light-absorbing species such as nitrate, nitrite and chromophoric dissolved organic matter (CDOM), which absorb sunlight and produce reactive transients ($^{\bullet}OH$, $CO_3^{-\bullet}$, $^1O_2$ and $^3CDOM^*$) that promote the degradation of xenobiotics. Note that xenobiotic degradation is in competition with deactivation processes of the transients, which include reaction with dissolved organic matter (DOM) for $^{\bullet}OH$ and $CO_3^{-\bullet}$, reaction with O_2 for $^3CDOM^*$, and thermal deactivation for both $^1O_2$ and $^3CDOM^*$. Photochemical reactions can be quite important, particularly for the transformation of biorecalcitrant compounds (Boreen et al., 2003; Canonica et al., 2005, 2006; Fenner et al., 2013; Bonvin et al., 2013; Remucal, 2014; Vione et al., in press).

In the present work, we evaluated the phototransformation of DMM in aqueous solution by combining a kinetic study of substrate degradation with a photochemistry model. The recently developed model can predict the photochemical transformation kinetics of organic pollutants in surface waters as a function of photoreactivity data and of key environmental variables, and it has been validated against field data (Maddigapu et al., 2011; Vione et al., 2011; De Laurentiis et al., 2012; Marchetti et al., 2013). The kinetic study was focused on DMM direct photolysis and on its reactivity towards the main transients that can be found in surface waters ($^{\bullet}OH$, $CO_3^{-\bullet}$, $^1O_2$ and $^3CDOM^*$). In addition, a survey was carried out of possible DMM phototransformation intermediates *via* the main photochemical pathways that would be operational in natural waters.

2. Experimental

2.1. Reagents and materials

Anthraquinone-2-sulphonic acid, sodium salt (AQ2S, 97%), furfuryl alcohol (98%), H_2O_2 (35%), $NaNO_3$ (>99%), $NaHCO_3$ (98%), anhydrous Na_2SO_4 (99%), NaCl (99.5%), $Na_2HPO_4 \cdot 2\ H_2O$ (98%), $NaH_2PO_4 \cdot H_2O$ (98%), $HClO_4$ (70%) and H_3PO_4 (85%) were purchased from Aldrich, dimethomorph (DMM, Pestanal analytical standard) from Fluka, NaOH (99%), propan-2-ol (LiChrosolv gradient grade) and dichloromethane (GC Suprasolv) from VWR Int., methanol (gradient grade) from Carlo Erba, Rose Bengal (RB) from Alfa Aesar.

2.2. Irradiation experiments

The reaction rate constant between DMM and $^{\bullet}OH$ was determined upon competition kinetics with propan-2-ol, using H_2O_2 under UVB irradiation as $^{\bullet}OH$ source (Wols and Hofman-Caris, 2012). A semi-quantitative assessment of the importance of the reaction between DMM and $CO_3^{-\bullet}$ was carried out upon UVB irradiation of nitrate and bicarbonate (Vione et al., 2009). Irradiated Rose Bengal (RB) was used as $^1O_2$ source (Garcia and Amat-Guerri, 2005) to study the rate constant of the relevant reaction with DMM, while anthraquinone-2-sulphonate (AQ2S) was used as triplet sensitiser (CDOM proxy to assess ^{3}CDOM* reactivity). The rationale for this choice is that quinones are common photoactive components of CDOM (Cory and McKnight, 2005). Moreover, irradiated AQ2S does not yield significant amounts of $^{\bullet}OH$ or $^1O_2$, differently from other triplet sensitisers, thereby reducing the importance of side reactions (Maddigapu et al., 2010; Bedini et al., 2012).

The choice of the irradiation devices for the different experiments depended on: *(i)* the absorption spectra of the target compounds (DMM or photosensitisers), measured with a Varian Cary 100 Scan double-beam UV-Vis spectrophotometer, using Hellma quartz cuvettes (1.000 cm optical path length), and *(ii)* the emission spectra of the lamps, recorded with an Ocean Optics USB 2000 CCD spectrophotometer (calibrated with an Ocean Optics DH-2000-CAL source). Solutions (5 mL total volume) were placed into cylindrical Pyrex glass cells (diameter 4.0 cm, height 2.5 cm), tightly closed with a lateral screw cap, and irradiated from the top under magnetic stirring. The incident UV irradiance on top of the solutions (290-400 nm) was measured with a power meter by CO.FO.ME.GRA. (Milan, Italy). The incident photon flux in solution was determined by ferrioxalate actinometry (Kuhn et al., 2004), by taking into account the wavelength trends of the actinometer absorption spectrum and of the photolysis quantum yield.

Three different lamps were used for the irradiation experiments: *(i)* a Philips TLK 05 UVA lamp with emission maximum at 365 nm, 24.0±1.5 W m^{-2} UV irradiance and $(1.82\pm0.23)\cdot10^{-5}$ Einstein L^{-1} s^{-1} incident photon flux, to study the direct photolysis of DMM and its reactivity with the AQ2S triplet state, ^{3}AQ2S*; *(ii)* a Philips TL 01 UVB lamp with emission maximum at 313 nm, 13.3±1.1 W m^{-2} UV irradiance and $(8.70\pm1.22)\cdot10^{-6}$ Einstein L^{-1} s^{-1} incident photon flux, to study reactivity with $^{\bullet}OH$ and $CO_3^{-\bullet}$; *(iii)* a Philips TL D 18W/16 yellow lamp with emission maximum at 545 nm and 10.3±0.9 W m^{-2} irradiance in the visible (measured with the CO.FO.ME.GRA. power meter equipped with a probe sensitive to visible radiation), to study the reaction with $^1O_2$ *via* Rose Bengal sensitisation. Figure 1 reports the emission spectra of the lamps (spectral photon flux densities, $p^{\circ}(\lambda)$) and the absorption spectra of the irradiated compounds (molar absorption coefficients, $\varepsilon(\lambda)$). Dark runs were carried out by wrapping the cells in aluminium foil and by placing them under the same lamps used for the irradiation experiments.

2.3. Analytical determinations

After the scheduled times, the cells were withdrawn from the lamps and the aqueous solutions underwent further processing. The monitoring of the time trend of DMM was carried out with a

VWR-Hitachi LaChrom Elite chromatograph equipped with L-2200 autosampler (injection volume 60 µL), L-2130 quaternary pump for low-pressure gradients, Duratec vacuum degasser, L-2300 column oven (set at 40°C), and L-2455 photodiode array detector. The column was a VWR LiChroCART 125-4 Cartridge, packed with LiChrospher 100 RP-18 (125mm×4 mm×5µm). The eluent (1.0 mL min^{-1} flow rate) was a mixture of methanol (A) and aqueous H_3PO_4 at pH 2.8 (B), with the following gradient: 10% A for 4 min, then to 65% A in 1 min and kept for 12 min, back to 10% A in 1 min and kept for 4 min (post-run equilibration). The detection wavelength was 220 nm. Commercial DMM is a mixture of two isomers (E and Z) and, coherently, injection of DMM stock solutions yielded two peaks at different retention times (13.9 and 15.0 min). The assignment of both peaks to the E and Z isomers of DMM was based on their chromatographic behaviour and on the photochemical inter-conversion patterns as known from the literature (*vide infra*).

The identification of DMM transformation intermediates was carried out by gas chromatography coupled with mass spectrometry. To this purpose, aqueous solutions after irradiation were extracted two times with 3 mL dichloromethane (the two extracts were then joined), dehumidified with anhydrous Na_2SO_4 and evaporated to dryness. Each sample was reconstructed with 100 µL dichloromethane. The solution was transferred into a vial and injected into a capillary gas chromatograph (Agilent 6890) coupled with a mass spectrometer (Agilent 5973 inert). The injection system used was a Gerstel CIS4 PTV. Initial injection temperature was 40 °C, programmed at 5 °C/s; final temperature was 320 °C, held for 9 min. The injection volume was 2 µL in the splitless mode. The capillary column used was a HP-5MS, 30 m × 0.25 mm × 0.25 µm film thickness. Initial column temperature was 40 °C and it was increased by 15 °C/min to 300 °C. The carrier gas was ultrapure He (1.0 mL/min; SIAD, Bergamo, Italy). The ionisation source worked in the electronic impact (EI) mode and the mass spectrometer worked in the Scan mode from 44 to 450 Th. Identification of the spectra was performed by using the Wiley 7n library (Agilent Part No. G1035B).

2.4. Kinetic data treatment

The E isomer of DMM undergoes rapid inter-conversion to the Z stereoisomer under UV irradiation (EPA, 1998; Lunn, 2007). Kinetic data of substrate transformation were derived by considering the time trend of the sum of both isomers, so that the E→Z photochemical conversion would not count as a net transformation of DMM. This choice was motivated by the fact that the sum of the two isomers followed pseudo-first order phototransformation kinetics with reasonable approximation, differently from the E and Z isomers taken separately. Therefore, the rates of the total (E + Z) DMM transformation were determined by fitting the relevant time evolution data with the equation $C_t\ C_o^{-1} = exp(-k\ t)$, where C_t is the concentration of (E+Z)DMM at the irradiation time t, C_o its initial concentration, and k the pseudo-first order degradation rate constant. The initial degradation rate was calculated as $R_{DMM} = k\ C_o$. The error bounds on R_{DMM} mainly depended on the uncertainty on k and they are reported as ± 1 standard deviation ($\mu \pm \sigma$). The reproducibility of repeated runs was

about 10-15%. Anyway, the monitoring of the time trends of both E-DMM and Z-DMM allowed an assessment of their respective reactivity after the very fast initial inter-conversion step.

2.5. Photochemical modelling

We have recently developed a model to predict the photochemical transformation kinetics of xenobiotics in surface waters. A detailed model description is provided in several previous publications (Maddigapu et al., 2011; Minella et al., 2013; De Laurentiis et al., 2014). Moreover, a software application was recently derived from the model (APEX: Aqueous Photochemistry of Environmentally-occurring Xenobiotics), which is available for free (including the User's Guide that contains a comprehensive account of model equations), as electronic supplementary information of Bodrato and Vione (2014) or at *http://chimica.campusnet.unito.it/do/didattica.pl/Quest?corso=7a3d*.

APEX predicts steady-state concentrations of $^{\bullet}OH$, $CO_3^{-\bullet}$, $^1O_2$ and ^{3}CDOM* based on water chemical composition and depth and on the spectral photon flux density of sunlight. It also predicts reaction kinetics (pseudo-first order rate constants) of pollutants with $^{\bullet}OH$, $CO_3^{-\bullet}$, $^1O_2$ and ^{3}CDOM*, as well as kinetics of direct photolysis. Required input data are pollutant absorption spectrum, photolysis quantum yield and second-order reaction rate constants with $^{\bullet}OH$, $CO_3^{-\bullet}$, $^1O_2$ and ^{3}CDOM*. The standardised time unit in the model is a summer sunny day (SSD), equivalent to fair-weather 15 July at 45°N latitude (Vione et al., 2011). By so doing, it is possible to take into account the day-night cycle and to use a time unit of definite duration that relates to outdoor conditions. The model results are average values over the water column of given depth, thus they take into account the higher photoactivity at the surface and the lower one at depth. They apply to well-mixed water bodies, including the epilimnion of stratified lakes.

An additional issue is that sunlight is not vertically incident over the water surface. The solar zenith angle should be considered, although refraction deviates the light path in water towards the vertical. Because of this phenomenon, the path length l of light in water is longer than the water depth d: on 15 July at 45°N it is $l = 1.05\ d$ at noon, and $l = 1.17\ d$ at ±3 h from noon that is a reasonable daily average.

3. Results and Discussion

3.1. Identification of the E and Z isomers of DMM

Under our analytical conditions DMM eluted as two separate peaks, hereafter labelled $DMM_{13.9}$ and $DMM_{15.0}$ based on retention time. Using HPLC elution on C18 material, shorter retention time has been found for the E isomer compared to the Z one (Takino and Sawada, 2010). Additional evidence was obtained upon UV irradiation of aqueous solutions of DMM. Our irradiation experiments showed a rapid decrease of the concentration of $DMM_{13.9}$ and a corresponding increase of $DMM_{15.0}$ (see Figure SM1 of the Supplementary Material to this paper, hereafter SM). The change in peak areas took place in less than 5 min under the adopted UVA and UVB devices (see Figure 1a,b for the lamp emission spectra), after which no further change took place for at least 30 min. The observed isomer conversion was a photoinduced reaction: the process kinetics were highly modified by using lamps having different emission spectra and, consequently, different overlap with the absorption spectrum of DMM. In contrast, the solution temperature (around 30°C) was similar in all the cases and the irradiance values were of the same order of magnitude. Compared to UVB and UVA irradiation, the isomer conversion was considerably slower (>3 h) under a Philips TLK 03 lamp with emission maximum at 430 nm (where DMM absorption is very limited), and it did not take place within 24 h under yellow-lamp irradiation, where DMM does not absorb at all (see Figure 1c for the spectrum of this lamp).

It is reported that the irradiation of DMM modifies the E:Z ratio from approximately 45:55 to around 25:75 or 20:80, after which the ratio of the isomers undergoes limited further changes (Lunn, 2007). Therefore, both chromatographic and photochemical considerations suggest that $DMM_{13.9}$ is the E isomer and $DMM_{15.0}$ the Z one.

3.2. Photochemical reactivity of DMM

In addition to the inter-conversion between the E and Z isomers (hereafter E-DMM and Z-DMM, respectively), net degradation of DMM intended as isomer mixture (DMM = E-DMM + Z-DMM) also took place under photochemical conditions. Transformation was studied for the sum of the two isomers, the time trend of which followed a pseudo-first order kinetics. The studied photochemical pathways were the direct photolysis and the reaction with photogenerated transients ($^{\bullet}OH$, $CO_3^{-\bullet}$, $^1O_2$ and $^3CDOM^*$, the latter assessed by using AQ2S as CDOM proxy). The experimental data are reported in the following section, while Table 1 summarizes the results concerning the direct photolysis quantum yield of DMM and the second-order reaction rate constants with the photoinduced transients under study. The values reported in Table 1 are lumped ones, because they are affected by the contributions of both DMM isomers.

In addition to the transformation of whole DMM, it is also interesting to have insight into the relative photostability/lability of its two isomers (E-DMM and Z-DMM). This issue is dealt with in

the Supplementary Material (Figure SM1). It was found that, after the fast initial inter-conversion, both E-DMM and Z-DMM showed comparable reactivity towards $^{\bullet}OH$ and $^{3}CDOM^{*}$ (the main transients that would be involved in the phototransformation of DMM in surface waters, *vide infra*).

3.3. Kinetics of DMM phototransformation

Direct photolysis. DMM (initial concentration 5 μM) was irradiated under the TLK 05 lamp (emission maximum at 365 nm, see Figure 1) at pH 7. Under these conditions the direct photolysis of DMM was limited and the initial transformation rate was $R_{DMM} = (1.29\pm0.15)\cdot10^{-12}$ M s^{-1} (μ±σ). The photon flux absorbed by DMM can be expressed as $P_a^{DMM} = \int_{\lambda} p°(\lambda)\,[1-10^{-\varepsilon_{DMM}(\lambda)b[DMM]}]d\lambda$ = $(4.94\pm0.62)\cdot10^{-8}$ Einstein L^{-1} s^{-1}, where $p°(\lambda)$ is the incident spectral photon flux density of the lamp, $\varepsilon_{DMM}(\lambda)$ the molar absorption coefficient of DMM (see Figure 1), b = 0.4 cm the optical path length in solution, and [DMM] = 5 μM. From these data it is possible to obtain the polychromatic photolysis quantum yield of DMM in the UVA region, where the spectra of the lamp and DMM overlap, as $\Phi_{DMM} = R_{DMM}\,(P_a^{DMM})^{-1} = (2.61\pm0.63)\cdot10^{-5}$. No dark transformation of DMM was observed at the time scale used for the irradiation experiments. Under irradiation, ~20% of the initial DMM was degraded in 7 days.

Reaction with $^{\bullet}OH$. The second-order reaction rate constant between DMM and $^{\bullet}OH$ was determined upon competition kinetics with propan-2-ol, using the UVB photolysis of H_2O_2 as $^{\bullet}OH$ source. Figure 2 reports the initial transformation rate of DMM (20 μM initial concentration) as a function of the concentration of propan-2-ol, upon irradiation with 1 mM H_2O_2. The transformation of DMM upon H_2O_2 photolysis would mainly involve the following reactions (Buxton et al., 1988):

$H_2O_2 + h\nu \rightarrow 2\ ^{\bullet}OH$		(1)
Propan-2-ol + $^{\bullet}OH \rightarrow$ Products	[$k_2 = 1.9\cdot10^9$ M^{-1} s^{-1}]	(2)
$H_2O_2 + {}^{\bullet}OH \rightarrow HO_2^{\bullet} + H_2O$	[$k_3 = 2.7\cdot10^7$ M^{-1} s^{-1}]	(3)
DMM + $^{\bullet}OH \rightarrow$ Products	[k_4]	(4)

The direct photolysis of DMM did not interfere significantly over an irradiation time scale of 4 h. Upon application of the steady-state approximation to $^{\bullet}OH$ one gets the following expression for R_{DMM}:

$$R_{DMM} = \frac{R_{\bullet OH}\cdot k_4\cdot[DMM]}{k_2\cdot[2-\text{Propanol}] + k_3\cdot[H_2O_2] + k_4\cdot[DMM]} \qquad (5)$$

The fit of the experimental data reported in Figure 2 with equation (5), using $R_{\bullet OH}$ = $(2.92\pm0.24)\cdot10^{-9}$ M s^{-1} (derived from the value of R_{DMM} without propan-2-ol) and with k_4 as floating variable yielded $k_4 = (2.56\pm0.44)\cdot10^{10}$ M^{-1} s^{-1} as the reaction rate constant between DMM

and $^{\bullet}OH$. Note that *(i)* 1 mM H_2O_2 would scavenge $^{\bullet}OH$ to a negligible extent compared to 20 µM DMM, and *(ii)* the reaction of DMM with the radical species formed from $^{\bullet}OH$ and propan-2-ol would be negligible, because $\lim_{[\text{Propan}-2-\text{ol}]\to\infty}(R_{DMM}) = 0$ (the trend of R_{DMM} *vs.* [Propan-2-ol] was not a plateau one).

Reaction with $CO_3^{-\bullet}$. Figure 3 reports the initial transformation rate of 20 µM DMM upon UVB irradiation of 10 mM $NaNO_3$, with the addition of variable $NaHCO_3$ concentrations. Because bicarbonate addition modifies the solution pH, the trend of R_{DMM} with irradiated nitrate is also shown in the presence of a phosphate buffer (NaH_2PO_4 + Na_2HPO_4) at the same concentration values as $NaHCO_3$ and same pH, within ±0.1 units. Finally, R_{DMM} in the presence of $NaHCO_3$ but without nitrate is also reported.

Figure 3 shows that: *(i)* DMM direct photolysis (irradiation without nitrate and in the presence of the non-absorbing HCO_3^-/CO_3^{2-} anions) was relatively low under the adopted experimental conditions (irradiation time up to 4h); *(ii)* DMM transformation with irradiated nitrate was little modified and even slightly inhibited by bicarbonate compared to the phosphate buffer.

The photolysis of nitrate yields photogenerated fragments inside a water cage ($[^{\bullet}OH + {}^{\bullet}NO_2]_{cage}$). The fragments can either recombine back to nitrate or diffuse into the solution bulk, where $^{\bullet}OH$ can react with dissolved substrates (Mark et al., 1996; Bouillon and Miller, 2005; Nissenson et al., 2010). The ions HCO_3^- and CO_3^{2-} can react with bulk $^{\bullet}OH$ to yield $CO_3^{-\bullet}$, which is considerably less reactive than the hydroxyl radical, but they could also react with cage $^{\bullet}OH$. This reaction would produce $CO_3^{-\bullet}$ and inhibit photofragment recombination to nitrate, as shown in the following reaction scheme:

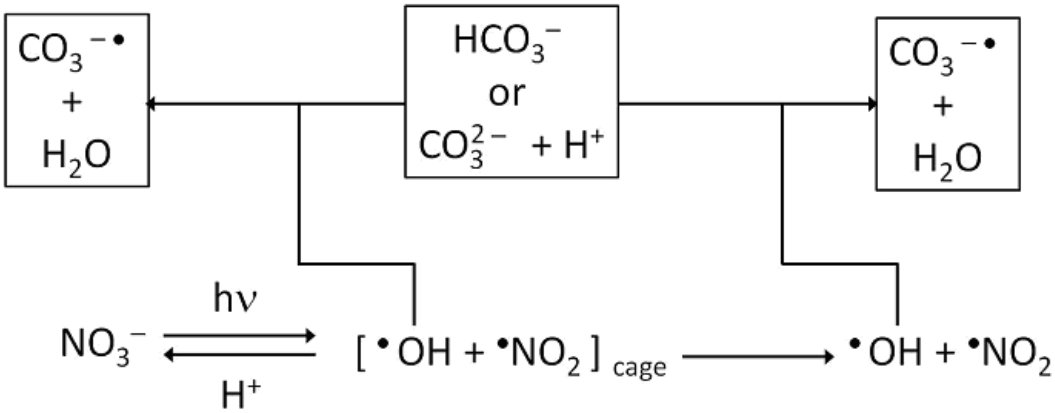

(6)

Because HCO_3^- and CO_3^{2-} inhibit the reaction of photofragment recombination, the formation rate of $CO_3^{-\bullet}$ in the presence of nitrate + bicarbonate would be significantly higher than the formation rate of $^{\bullet}OH$ with nitrate alone. The formation of a higher amount of a less reactive species has variable effects depending on the reactivity of a dissolved substrate with $CO_3^{-\bullet}$ *vs.* $^{\bullet}OH$. The degradation of compounds that are poorly reactive toward $CO_3^{-\bullet}$, and that would also undergo insignificant transformation by $CO_3^{-\bullet}$ in surface waters, would be inhibited by bicarbonate.

Conversely, the degradation of compounds that react with $CO_3^{-\bullet}$ to a significant extent would be enhanced by bicarbonate (Vione et al., 2009; De Laurentiis et al., 2014). In the case of DMM, the results reported in Figure 3 show that the reaction rate in the presence of HCO_3^-/CO_3^{2-} was slightly lower than that in the presence of the phosphate buffer. Therefore, it is suggested that $CO_3^{-\bullet}$ would not play a significant role in the degradation of DMM in surface-water environments.

Reaction with $^1O_2$. This reaction was studied upon irradiation (yellow lamp) of DMM with 10 μM Rose Bengal (RB) as source of $^1O_2$. The reaction (8) between DMM and $^1O_2$ would be in competition with the thermal deactivation of singlet oxygen (reaction (9); Rodgers and Snowden, 1982):

$RB + h\nu + O_2 \rightarrow RB + {}^1O_2$		(7)
$DMM + {}^1O_2 \rightarrow$ Products	[k_8]	(8)
${}^1O_2 \rightarrow O_2 + $ heat	[$k_9 = 2.5 \cdot 10^5$ s^{-1}]	(9)

Upon application of the steady-state approximation to $^1O_2$ one gets the following expression for R_{DMM}:

$$R_{DMM} = \frac{R_{^1O_2} \cdot k_8 \cdot [DMM]}{k_9 + k_8 \cdot [DMM]} \quad (10)$$

where $R_{^1O_2}$ is the formation rate of $^1O_2$ by 10 μM RB under the adopted irradiation device. At very low DMM it would be k_8 [DMM] « k_9, and the equation (10) would be linearised as $R_{DMM} = R_{^1O_2} \cdot k_8 \cdot k_9^{-1} \cdot [DMM]$. Coherently, the experimental trend of R_{DMM} *vs.* [DMM] was linear (see Figure SM2) and it could be fitted with $R_{DMM} = (1.21 \pm 0.04) \cdot 10^{-6}$ [DMM].

The measurement of $R_{^1O_2}$ was carried out upon irradiation of 10 μM RB + 0.1 mM furfuryl alcohol (FFA), which reacts with $^1O_2$ with rate constant $k_{FFA} = 7.8 \cdot 10^8$ M^{-1} s^{-1} (Wilkinson and Brummer, 1981). The initial transformation rate of FFA, experimentally determined, was $R_{FFA} = (8.46 \pm 0.11) \cdot 10^{-8}$ M s^{-1}. Photogenerated $^1O_2$ could undergo deactivation or reaction with FFA, and upon application of the steady-state approximation to [$^1O_2$] one obtains:

$$R_{^1O_2} = R_{FFA} \cdot \frac{k_9 + k_{FFA} \cdot [FFA]}{k_{FFA} \cdot [FFA]} \quad (11)$$

From equation (11) one gets $R_{^1O_2} = (3.56 \pm 0.05) \cdot 10^{-7}$ M s^{-1}. With this value and by comparison between equation (10) (linearised form) and the experimental data one obtains $R_{^1O_2} \cdot k_8 \cdot k_9^{-1} = (1.21 \pm 0.04) \cdot 10^{-6}$, from which $k_8 = (8.50 \pm 0.28) \cdot 10^5$ M^{-1} s^{-1} is derived as the reaction rate constant

between DMM and $^1O_2$. This rate constant is quite low, thus the $^1O_2$ pathway is unlikely to play a significant role in the transformation of DMM.

Reaction with irradiated AQ2S. The UVA irradiation of DMM with 0.1 mM AQ2S was used to measure the reaction rate constant between DMM and ^{3}AQ2S*. The (linear) trend of R_{DMM} *vs.* [DMM] under these conditions is reported in Figure SM3 and the relevant data fit yielded R_{DMM} = (3.96±0.28)·10^{-5} [DMM].

Both AQ2S and DMM absorb lamp radiation. From the Lambert-Beer approach (Kuhn et al., 2004) one derives that $p_a^{AQ2S}(\lambda)\cdot\left(p_a^{DMM}(\lambda)\right)^{-1} = A_{AQ2S}(\lambda)\cdot\left(A_{DMM}(\lambda)\right)^{-1}$, where $A_{DMM}(\lambda)$ and $A_{AQ2S}(\lambda)$ are the absorbance values of DMM and AQ2S at the wavelength λ, and $p_a^{DMM}(\lambda)$, $p_a^{AQ2S}(\lambda)$ are the respective values of the absorbed spectral photon flux density. Competition for lamp irradiance between DMM and AQ2S has limited impact on radiation absorption by AQ2S: the absorbed photon flux P_a^{AQ2S} would be decreased by less than 1% when passing from 0.1 mM AQ2S alone to 0.1 mM AQ2S + 15 µM DMM, the highest tested DMM concentration. Therefore, with very good approximation one can simply determine $P_a^{AQ2S} = \int_\lambda p_a^{AQ2S}(\lambda)\,d\lambda$ = (1.54±0.04)·10^{-6} Einstein L^{-1} s^{-1}, where $p_a^{AQ2S}(\lambda) = p°(\lambda)[1-10^{-\varepsilon_{AQ2S}(\lambda)b[AQ2S]}]$ ($p°(\lambda)$ is the spectral incident photon flux density of the UVA lamp, reported in Figure 1a, b = 0.4 cm is the optical path length in the experimental cells, and [AQ2S] = 0.1 mM).

The reactive triplet state ^{3}AQ2S* accounts for the degradation processes that take place with AQ2S under irradiation. It has formation quantum yield $\phi_{^3AQ2S^*}$ = 0.18 and deactivation rate constant $k_{^3AQ2S^*}$ = 1.1·10^7 s^{-1} (Loeff and Treinin, 1983). The formation rate of ^{3}AQ2S* is $R_{^3AQ2S^*}$ = $\phi_{^3AQ2S^*}$ P_a^{AQ2S}, and its deactivation would compete with the reaction with DMM (rate constant $k_{^3AQ2S^*,DMM}$). Therefore, the transformation rate of DMM by irradiated AQ2S could be expressed as follows:

$$R_{DMM} = \phi_{^3AQ2S^*}\cdot P_a^{AQ2S}\cdot\frac{k_{^3AQ2S^*,DMM}\cdot[DMM]}{k_{^3AQ2S^*}+k_{^3AQ2S^*,DMM}\cdot[DMM]} \qquad (12)$$

Under the hypothesis that $k_{^3AQ2S^*,DMM}$ [DMM] « $k_{^3AQ2S^*}$, one gets R_{DMM} = $\phi_{^3AQ2S^*}$ P_a^{AQ2S} $k_{^3AQ2S^*,DMM}$ $(k_{^3AQ2S^*})^{-1}$ [DMM], which would be compatible with the experimentally observed linear trend (R_{DMM} = (3.96±0.28)·10^{-5} [DMM]). By application of the linearised form of equation (12) to the experimental data, one gets $\phi_{^3AQ2S^*}$ P_a^{AQ2S} $k_{^3AQ2S^*,DMM}$ $(k_{^3AQ2S^*})^{-1}$ = (3.96±0.28)·10^{-5} and, as a consequence, $k_{^3AQ2S^*,DMM}$ = (1.57±0.15)·10^9 M^{-1} s^{-1} as the second-order reaction rate constant between ^{3}AQ2S* and DMM. This finding confirms that the hypothesis $k_{^3AQ2S^*,DMM}$

[DMM] « $k_{^3AQ2S^*}$ was reasonable. Hereafter, it will be assumed that the value of $k_{^3AQ2S^*,DMM}$ is representative of the reaction rate constant(s) between DMM and ^{3}CDOM*.

3.4. DMM transformation intermediates

The study of the intermediates formed by substrate irradiation is important, because some of them could be more harmful than the parent compounds (Donner et al., 2013). To facilitate intermediate identification, irradiation of saturated solutions of DMM was carried out (concentration around 0.1 mM). The studied systems were DMM alone (direct photolysis), DMM + H_2O_2 ($^{\bullet}$OH pathway), and DMM + AQ2S (^{3}CDOM* pathway). The photochemical pathways that are almost certainly negligible ($CO_3^{-\bullet}$ and $^1O_2$) were no longer studied.

It was not possible to detect DMM intermediates upon direct photolysis or irradiation with 1 mM H_2O_2, probably because even with a saturated aqueous solution of DMM (the solubility of which in water is however limited), the intermediates had lower concentration values than the limit of detection of the analytical methodology. In fact, if the intermediates are degraded faster than the parent compound, their concentrations in the studied systems may be extremely low. In contrast, three potentially important intermediates could be identified upon irradiation of DMM with 1 mM AQ2S. These intermediates are N-formylmorpholine (*m/z* = 115), 4-chloroacetophenone (*m/z* = 154) and 4-chlorobenzoic acid (*m/z* = 156) (see Table 2). The experimental mass spectra, obtained by means of GC-MS analysis, and the comparison with the spectra libraries are reported in the SM (Figures SM4-SM6). Interestingly, 4-chlorobenzoic acid and 4-chloroacetophenone accumulated in the system up to the longest irradiation time tested (8 h), while N-formylmorpholine peaked at low irradiation time.

The formation of N-formylmorpholine has been hypothesised by Al Rashidi et al. (2013, 2014), who investigated the transformation of DMM in the gas phase by ozonolysis and reaction with $^{\bullet}$OH (produced by photolysis of gaseous HONO). The only identified intermediate (by GC-MS) was in both cases the (4-chlorophenyl)(3,4-dimethoxyphenyl)methanone (CPMPM). In the presence of ozone, the cleavage of the double bond would yield several compounds, including CPMPM and unstable Criegee intermediates. Some of the latter may undergo degradation to produce N-formylmorpholine. The reaction with $^{\bullet}$OH would also cause the cleavage of the double bond, producing CPMPM and a morpholinic glyoxal that could be transformed into N-formylmorpholine by CO loss. The main reactive species with irradiated AQ2S is ^{3}AQ2S*, which can simulate the $^{\bullet}$OH reactivity in some cases (Vione et al., 2010; Bedini et al., 2012). However, ^{3}AQ2S* can also produce different intermediates than $^{\bullet}$OH, or the same intermediates with different yields (Vione et al., 2011; De Laurentiis et al., 2012, 2014).

N-Formylmorpholine is a solvent of low toxicity, and the lethal dose for rats is 6500 mg kg^{-1} (Lewis, 1992). It is, therefore, slightly less toxic than DMM, the lethal dose of which for rats is 3900 mg kg^{-1} (EPA, 1998; Lunn, 2007). From these data one can infer that the transformation of DMM into N-formylmorpholine could slightly reduce the system toxicity, at least for mammals.

The other two intermediates are also commonly found in industrial wastes (D'Oliveira et al., 1993, Shimizu et al., 2005, Mhemdi et al., 2013). The acute toxicity of 4-chlorobenzoic acid for rats is quite comparable to that of N-formylmorpholine (TCI, 2005), while 4-chloroacetophenone is very toxic by inhalation but much less dangerous by ingestion (the lethal dose for rats by oral intake is above 2000 mg kg^{-1}; Merck-Millipore, 2011). Compared to the parent DMM, and considering that the detected intermediates would be formed in water bodies, it does not seem that they could cause acute toxicity concerns for mammals, with the possible exception of the (presumably rare) cases where 4-chloroacetophenone may be inhaled. Unfortunately, no data are available about possible long-term effects. The acute toxicity for aquatic organisms is probably more environmentally significant than that for mammals, given the expected harmful effects of DMM. In this context, the detected intermediates should be less toxic than DMM towards fish, invertebrates and algae (EPA, 1998; BASF, 2008; Merck-Millipore, 2010, 2011). Therefore, photodegradation of DMM by ^{3}CDOM* could reduce its acute impact on aquatic environments.

3.5. Photochemical modelling

Based on the data reported in Table 1, the expected photochemical persistence of DMM in surface waters was modelled with the APEX software. Figure 4A reports the half-life time of DMM as a function of the optical path length of sunlight in water (which is proportional to the water depth, see section 2.5) and of the dissolved organic carbon (DOC, units of mg C L^{-1}). Other (fixed) water conditions are 0.1 mM nitrate, 1 µM nitrite, 1 mM bicarbonate and 10 µM carbonate. Note that, within APEX, DOC is used as a measure of both DOM and CDOM. Under such circumstances the half-life time of DMM (referred to fair-weather summertime) would vary from a few days to over one month. In particular, $t_{½}$ would increase with increasing path length because the bottom layers of a deep water body are poorly illuminated by sunlight. Furthermore, increasing DOC causes the $t_{½}$ to increase, because DOM efficiently scavenges $^{\bullet}$OH and inhibits an important pathway of DMM transformation. The inhibition of $^{\bullet}$OH reactions by DOM is only partially offset by the enhancement of the ^{3}CDOM*-induced processes at high DOC. Under the reported conditions, the $^{\bullet}$OH pathway would in fact prevail at low DOC and the ^{3}CDOM* reactions at high DOC, while the relative importance of the direct photolysis would be <10% (see Figure 5, which shows the fraction of DMM degraded by $^{\bullet}$OH (A), ^{3}CDOM* (B) and the direct photolysis (C) in the considered conditions).

Nitrate and nitrite can be important $^{\bullet}$OH sources in surface waters. The values of [NO_3^-] and [NO_2^-] used for the calculations in Figure 4A (0.1 mM and 1 µM, respectively) are fairly high (Longhi et al., 2013). Figure 4B reports the $t_{½}$ of DMM in the presence of 1 µM nitrate and 10 nM nitrite (which could be representative of a hypereutrophic water body during elevated productivity periods; Pinardi et al., 2011), and otherwise identical conditions as for Figure 4A. Limited difference between the $t_{½}$ values of Figure 4A and 4B can be seen at high DOC and high path length, where DMM transformation would mainly occur upon reaction with ^{3}CDOM* (see Figure

5). In contrast, the $t_{½}$ values are quite different at low DOC and low path length. Under such circumstances the transformation reactions involving $^{\bullet}OH$ would be important (Figure 5) and they are enhanced in the presence of elevated nitrate and nitrite. The photochemistry of these nitrogen species is more important in shallow waters because nitrate mainly absorbs UVB and nitrite UVA radiation, the column penetration of which is lower compared to *e.g.* visible light (Loiselle et al., 2008). The decrease of $t_{½}$ with increasing DOC at low path length, shown in Figure 4B is due to the fact that because of low nitrite and nitrate, the role of CDOM as source of $^{3}CDOM^{*}$ and most notably $^{\bullet}OH$ is more important than that of DOM as $^{\bullet}OH$ sink.

The modelled half-life times of Figure 4 are referred to summertime irradiation conditions. The *APEX_Season* function of the APEX software can give insight into the photochemical reaction kinetics in different seasons. Figure 6 reports the monthly trend of the $t_{½}$ of DMM (with nitrate and nitrite as per Figure 4A, for other conditions see the figure caption), showing a variation from ~10 days in summer to 60-90 days in winter. The error bars shown on the plot ($\pm\sigma$) represent the model uncertainty and they were calculated with the *APEX_Errors* function of APEX.

4. Conclusions

Commercial DMM is a mixture of two isomers (E and Z), which undergo very rapid E $\rightarrow$ Z interconversion under UV irradiation. The DMM (intended as the sum of the two isomers) also undergoes photodegradation, although with a longer time scale. The modelled photochemical half-life time of DMM would range from about a week to several months in surface-water environments, depending on environmental conditions such as water chemistry, depth and seasonality. In particular, photodegradation would be favoured in shallow waters with low DOC during the summer season. If, additionally, nitrate and nitrite reach elevated levels, the half-life time could be even decreased to a few days. To our knowledge, this is the first assessment ever carried out of the photochemical half-life time of DMM in surface water bodies. For lifetimes of a few weeks or shorter, photochemistry would be a key issue in DMM transformation in environmental waters.

The main photochemical pathways accounting for DMM degradation would be $^{\bullet}OH$ in DOM-poor waters (low DOC) and $^{3}CDOM^{*}$ in DOM-rich ones (high DOC). In contrast, direct photolysis would play a secondary role. Additional processes (reaction with $^{1}O_2$ and $CO_3^{-\bullet}$) can be safely neglected. Interestingly, after the very fast E $\rightarrow$ Z interconversion, the E and Z isomers showed comparable reactivity with $^{\bullet}OH$ and $^{3}CDOM^{*}$.

In the case of reaction with $^{3}CDOM^{*}$ (studied by using AQ2S as CDOM proxy), the compounds N-formylmorpholine, 4-chloroacetophenone and 4-chlorobenzoic acid were identified as DMM transformation intermediates. Their acute toxicity for rats is grossly comparable to that of DMM, allowing the inference that the $^{3}CDOM^{*}$ pathway would not lead to an increase of acute toxicity for mammals. A partial exception might be represented by scenarios in which 4-chloroacetophenone may be inhaled, because the toxicity of this compound by inhalation is much

higher compared to ingestion or dermal contact. Interestingly, the detected intermediates are less toxic than DMM towards aquatic organisms (fish, invertebrates, algae). By combining the toxicity data reported in the literature and the experimental evidence here detailed, one can infer that the ^{3}CDOM* pathway might reduce the adverse effects of DMM on aquatic ecosystems.

Acknowledgements

DV acknowledges financial support from Università di Torino - EU Accelerating Grants, project TO_Call2_2012_0047 (Impact of radiation on the dynamics of dissolved organic matter in aquatic ecosystems - DOMNAMICS). The DOMNAMICS project also supported PA's post-doc fellowship. EDL's PhD grant was financially supported by Fondazione CRT - Progetto Lagrange (Torino, Italy). GM's bursary was supported by Fondazione CRT - Borse Lagrange di Ricerca Applicata. The authors are grateful to Riccardo Ariotti (owner of LAV s.r.l.) for co-financing GM's bursary and for his support.

References

Albert G, Curtze, J, Drandarevski CHA. Dimethomorph (CME 151), a novel curative fungicide. Brighton Crop Prot Conf-Pests Dis 1988;1: 17-21.

Baby UI, Ajay D, Premkumar R. Combined use of morpholine and triazole fungicides for the management of blister blight of tea. Trop Agric 2004;81:49–53.

BASF (Badische Anilin und Soda Fabrik). Material Safety Data Sheet (MSDS), N-formylmorpholine, 2010. *http://worldaccount.basf.com*, last accessed July 2014.

Bedini A, De Laurentiis E, Sur B, Maurino V, Minero C, Brigante M, Mailhot G, Vione D. Phototransformation of anthraquinone-2-sulphonate in aqueous solution. Photochem Photobiol Sci 2012;11:1445-53.

Bodrato M, Vione D. APEX (Aqueous Photochemistry of Environmentally occurring Xenobiotics): A free software tool to predict the kinetics of photochemical processes in surface waters. Environ Sci: Processes Impacts 2014;16:732-40.

Bonvin F, Razmi A, Barry DA, Kohn T. Micropollutant dynamics in Vidy Bay - A coupled hydrodynamic-photolysis model to assess the spatial extent of ecotoxicological risk. Environ Sci Technol 2013;47:9207-16.

Boreen AL, Arnold WA, McNeill K. Photodegradation of pharmaceuticals in the aquatic environment: A review. Aquat. Sci. 2003;65:320-41.

Bouillon RC, Miller WL. Photodegradation of dimethyl sulfide (DMS) in natural waters: Laboratory assessment of the nitrate-photolysis-induced DMS oxidation. Environ Sci Technol 2005;39:9471-7.

Buxton GV, Greenstock CL, Helman WP, Ross AB. Critical review of rate constants for reactions of hydrated electrons, hydrogen atoms and hydroxyl radicals ($^{\bullet}OH/^{\bullet}O^{-}$) in aqueous solution. J Phys Chem Ref Data 1988;17:1027-284.

Calza P, Massolino C, Pelizzetti E. Photo-induced transformation of hexaconazole and dimethomorph over TiO_2 suspension. J Photoch Photobio A 2008;200:356-63.

Canonica S, Kohn T, Mac M, Real FJ, Wirz J, Von Gunten U. Photosensitizer method to determine rate constants for the reaction of carbonate radical with organic compounds. Environ Sci Technol 2005;39:9182-8.

Canonica S, Hellrung B, Müller P, Wirz J. Aqueous oxidation of phenylurea herbicides by triplet aromatic ketones. Environ Sci Technol 2006;40:6636-41.

Cory RM, McKnight DM. Fluorescence spectroscopy reveals ubiquitous presence of oxidized and reduced quinones in dissolved organic matter. Environ Sci Technol 2005;39:8142-9.

D'Oliveira JC, Jayatilake WDW, Tennakone K, Herrmann JM, Pichat P. Heterogeneous photocatalysis as a method of water decontamination - degradation of 2-chlorobenzoic, 3-chlorobenzoic and 4-chlorobenzoic acids over illuminated TiO_2 at room-temperature. Stud Surf Sci Catal 1993;75:2167–71.

De Laurentiis E, Chiron S, Kouras-Hadef S, Richard C, Minella M, Maurino V, Minero C, Vione D. Photochemical fate of carbamazepine in surface freshwaters: Laboratory measures and modeling. Environ Sci Technol 2012;46:8164-73.

De Laurentiis E, Prasse C, Ternes TA, Minella M, Maurino V, Minero C, Sarakha M, Brigante M, Vione D. Assessing the photochemical transformation pathways of acetaminophen relevant to surface waters: Transformation kinetics, intermediates, and modelling. Wat Res 2014;53:235-48.

Donner E, Kosjek T, Qualmann S, Kusk KO, Heath E, Revitt DM, Ledin A, Andersen HR. Ecotoxicity of carbamazepine and its UV photolysis transformation products. Sci Total Environ 2013;443:870-6.

EPA (Environmental Protection Agency). Pesticide Fact Sheet: Dimethomorph. Arlington, VA, 1998.

Fenner K, Canonica S, Wackett LP, Elsner M. Evaluating pesticide degradation in the environment: Blind spots and emerging opportunities. Science 2013;341:752-8.

Fluka. Material Safety Data Sheet (MSDS), dimethomorph. *http://www.sigmaaldrich.com*, last accessed July 2014.

Garcia NA, Amat-Guerri F. Photodegradation of hydroxylated N-hetero aromatic derivatives in natural-like aquatic environments - A review of kinetic data of pesticide model compounds. Chemosphere 2005;59:1067-82.

Knoch E, Holman JC. Dimethomorph (AC 336379): Determination of the direct phototransformation in buffered medium at pH 7. Institut Fresenius Gruppe Isotope Laboratory; Herten; Germany Fed.Rep.. BASF Document No. DK-324-004. Unpublished. BASF 1998 (cited by Lunn, 2007. Original document not available).

Kuhn HJ, Braslavsky SE, Schmidt R. Chemical actinometry. Pure Appl Chem 2004;76:2105-46.

Liu CY, Wan K, Huang JX, Wang YC, Wang FH. Behavior of mixed formulation of metalaxyl and dimethomorph in grape and soil under field conditions. Ecotoxicol Environ Saf 2012;84:112-6.

Lewis RJ. Sax's Dangerous Properties of Industrial Materials. 8th ed. New York: Van Nostrand Reinhold; 1992.

Loeff I, Treinin A, Linschitz H. Photochemistry of 9,10-anthraquinone-2-sulfonate in solution. 1. Intermediates and mechanism. J Phys Chem 1983;87:2536-44.

Loiselle SA, Azza N, Cozar A, Bracchini L, Tognazzi A, Dattilo A, Rossi, C. Variability in factors causing light attenuation in Lake Victoria. Freshw Biol 2008;53:535-45.

Longhi D, Bartoli M, Nizzoli D, Viaroli P. Benthic processes in fresh water fluffy sediments undergoing resuspension. J Limnol 2013;72:1-12.

Lunn D. Dimethomorph. Food and Agriculture Organization of the United Nations, 2007 (140 pp).

Maddigapu PR, Bedini A, Minero C, Maurino V, Vione D, Brigante M, Mailhot G, Sarakha M. The pH-dependent photochemistry of anthraquinone-2-sulfonate. Photochem Photobiol Sci 2010;9:323-30.

Maddigapu PR, Minella M, Vione D, Maurino V, Minero C. Modeling phototransformation reactions in surface water bodies: 2,4-Dichloro-6-nitrophenol as a case study. Environ Sci Technol 2011;45:209-14.

Maillard E, Payraudeau S, Faivre E, Grégoire C, Gangloff F, Imfeld G. Removal of pesticide mixtures in a stormwater wetland collecting runoff from a vineyard catchment. Sci Total Environ 2011;409:2317-24.

Marchetti G, Minella M, Maurino V, Minero C, Vione D. Photochemical transformation of atrazine and formation of photointermediates under conditions relevant to sunlit surface waters: Laboratory measures and modelling. Wat Res 2013;47:6211-22.

Mark G, Korth HG, Schuchmann HP, von Sonntag C. The photochemistry of aqueous nitrate ion revisited. J Photochem Photobiol A: Chem 1996;101:89-103.

Merck-Millipore. Material Safety Data Sheet (MSDS), 2-chlorobenzoic acid, 2010. *https://it.vwr.com*, last accessed July 2014.

Merck-Millipore. Material Safety Data Sheet (MSDS), 4-chloroacetophenone, 2011. *https://it.vwr.com*, last accessed July 2014.

Mhemdi A, Oturan MA, Oturan N, Abdelhedi R, Ammar S. Electrochemical advanced oxidation of 2 -chlorobenzoic acid using BDD or Pt anode and carbon felt cathode. J Electroanal Chem 2013;709:111-7.

Minella M, De Laurentiis E, Buhvestova O, Haldna M, Kangur K, Maurino V, Minero C, Vione, D. Modelling lake-water photochemistry: Three-decade assessment of the steady-state concentration of photoreactive transients ($^{\bullet}OH$, $CO_3^{-\bullet}$ and $^3CDOM^*$) in the surface water of polymictic Lake Peipsi (Estonia/Russia). Chemosphere 2013;90:2589-96.

Nissenson P, Dabdub D, Das R, Maurino V, Minero C, Vione D. Evidence of the water-cage effect on the photolysis of NO_3^- and $FeOH^{2+}$. Implications of this effect and of H_2O_2 surface

accumulation on photochemistry at the air-water interface of atmospheric droplets. Atmos Environ 2010;44:4859-66.

Oliveira T, Becker H, Longhinotti E, De Souza D, de Lima-Neto P, Correia, AN. Carbon-fibre microelectrodes coupled with square-wave voltammetry for the direct analysis of dimethomorph fungicide in natural waters. Microchem J 2013;109:84-92.

Panek MG et al (unspecified). Aqueous Photolysis of 14C-BAS 550 F. BASF AG; Ludwigshafen/Rhein; Germany Fed. Rep. BASF Document No. DK-324-006. Unpublished. BASF 2001. (cited by Lunn, 2007. Original document not available).

Pinardi M, Bartoli M, Longhi D, Viaroli P. Net autotrophy in a fluvial lake: the relative role of phytoplankton and floating-leaved macrophytes. Aquat Sci 2011;73:389-403.

Rashidi AM, Chakir A, Roth E. Heterogeneous ozonolysis of folpet and dimethomorph: A kinetic and mechanistic study. J Phys Chem A 2013;117:2908-15.

Rashidi AM, Chakir, A, Roth E. Heterogeneous oxidation of folpet and dimethomorph by OH radicals: A kinetic and mechanistic study, Atmos Environ 2014;82:164-71.

Remucal CK. The role of indirect photochemical degradation in the environmental fate of pesticides: A review. Environ Sci: Processes Impacts 2014;16:628-53.

Rodgers MAJ, Snowden PT. Lifetime of $^1O_2$ in liquid water as determined by time-resolved infrared luminescence measurements. J Am Chem Soc 1982;104:5541-3.

Shimizu, K, Murayama H, Nagai A, Shimada A, Hatamachi T, Kodama T, Kitayama Y. Degradation of hydrophobic organic pollutants by titania pillared fluorine mica as a substrate specific photocatalyst. Appl Catal B-Environ 2005;55:141-8.

Stein JM, Kirk WW. Field optimization of dimethomorph for the control of potato late blight Phytophthora infestans: application rate, interval, and mixtures. Crop Prot 2003;22:609-14.

Takino M, Sawada H. Comprehensive screening of pesticides by LC/TOFMS. Proceedings of EPRW2010 (European Pesticides Residues Workshop), Strasbourg, France, 20-24 June 2010. *http://www.eprw2010.com*, last accessed July 2010.

TCI (Tokyo Chemical Industry) America. Material Safety Data Sheet (MSDS), N-formylmorpholine, 2005. *http://www.tcichemicals.com*, last accessed July 2014.

Van Dijk A. Photodegradation study of 14-C Dimethomorph (CME 151) in water. RCC Umweltchemie AG; Itingen; Switzerland. BASF Document No. DK-630-001. Unpublished. BASF, 1990. (cited by Lunn, 2007. Original document not available).

Vione D, Khanra S, Cucu Man S, Maddigapu PR, Das R, Arsene C, Olariu RI, Maurino V, Minero C. Inhibition vs. enhancement of the nitrate-induced phototransformation of organic substrates by the $^{\bullet}OH$ scavengers bicarbonate and carbonate. Wat Res 2009;43:4718-28.

Vione D, Ponzo M, Bagnus D, Maurino V, Minero C, Carlotti ME. Comparison of different probe molecules for the quantification of hydroxyl radicals in aqueous solution. Environ Chem Lett 2010;8:95-100.

Vione D, Maddigapu PR, De Laurentiis E, Minella M, Pazzi M, Maurino V, Minero C, Kouras S, Richard C. Modelling the photochemical fate of ibuprofen in surface waters. Wat Res 2011;45:6725-36.

Vione D, Minella M, Maurino V, Minero C. Indirect photochemistry in sunlit surface waters : Photoinduced production of reactive transient species. Chemistry Eur J, in press. DOI: 10.1002/chem.201400413.

Wicks T, Hall B. Efficacy of dimethomorph (CME151) against downy mildew of grapevines. Plant Dis 1990; 74:114-6.

Wilkinson F, Brummer J. Rate constants for the decay and reactions of the lowest electronically excited singlet-state of molecular oxygen in solution. J Phys Chem Ref Data 1981;10:809-1000.

Wols BA, Hofman-Caris CHM. Review of photochemical reaction constants of organic micropollutants required for UV advanced oxidation processes in water. Wat Res 2012;46: 2815-27.

Yan, JH, Huang KL, Liu SQ, Zeng HZ. Photocatalytic degradation of dimethomorph on nanometer titanium dioxide by silver depositing in aqueous suspension. Trans Nonferrous Met Soc China 2005;15:680-5.

Table 1. Photochemical kinetic parameters of DMM (sum of E and Z isomers). AQ2S was used as proxy of CDOM. The reaction between DMM and $CO_3^{-\bullet}$ would not be significant in environmental waters. The structures of the E and Z isomers of DMM are also reported.

Photochemical pathway	***Parameter***	***Value ($\mu\pm\sigma$)***
Direct photolysis	Φ_{DMM}	$(2.61\pm0.63)\cdot10^{-5}$
Reaction with $^{\bullet}OH$	$k_{^{\bullet}OH,DMM}$	$(2.56\pm0.44)\cdot10^{10}$ M^{-1} s^{-1}
Reaction with $^1O_2$	$k_{^1O_2,DMM}$	$(8.50\pm0.28)\cdot10^{5}$ M^{-1} s^{-1}
Reaction with $^3CDOM^*$	$k_{^3AQ2S^*,DMM}$	$(1.57\pm0.15)\cdot10^{9}$ M^{-1} s^{-1}

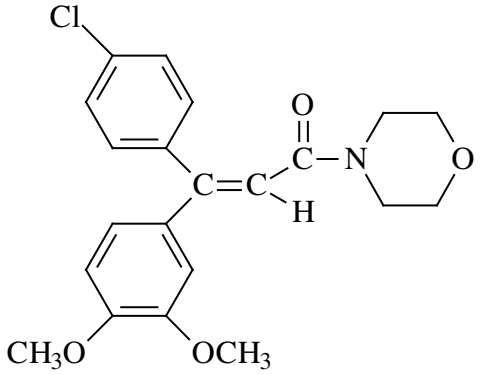

E-DMM

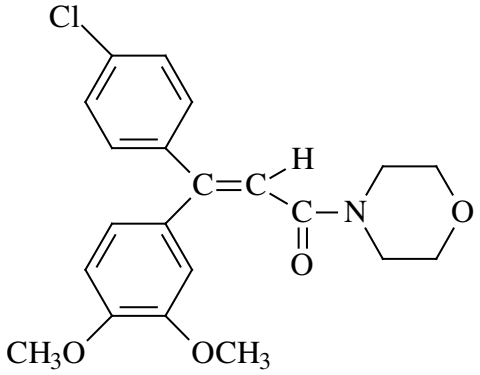

Z-DMM

Table 2. DMM intermediates, identified by GC-MS upon UVA irradiation in the presence of AQ2S. Further information on their identification is provided as SM.

Compound	*Structural Formula*	*m/z*	t_R, *min*
1-Formylmorpholine	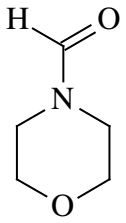	115	4.61
4-Chloroacetophenone	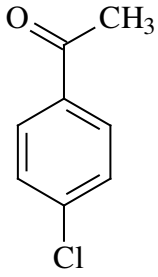	154	5.72
4-Chlorobenzoic acid	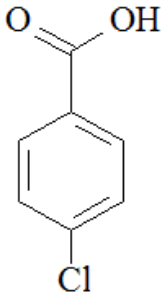	156	7.21

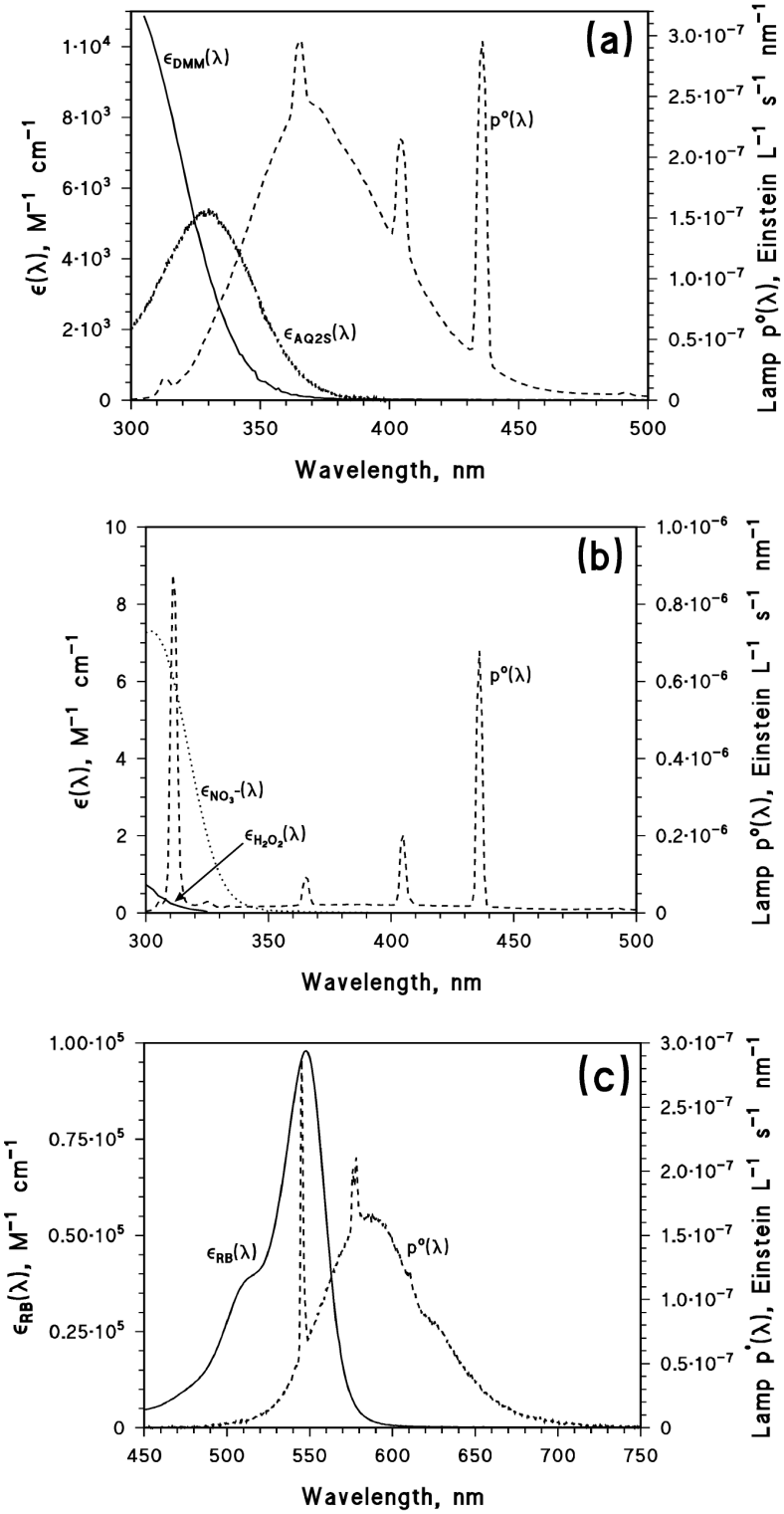

Figure 1. Absorption (molar absorption coefficients) and emission spectra (spectral photon flux densities) of: **(a)** UVA lamp, DMM and AQ2S; **(b)** UVB lamp, H_2O_2 and nitrate; **(c)** yellow lamp and Rose Bengal (RB).

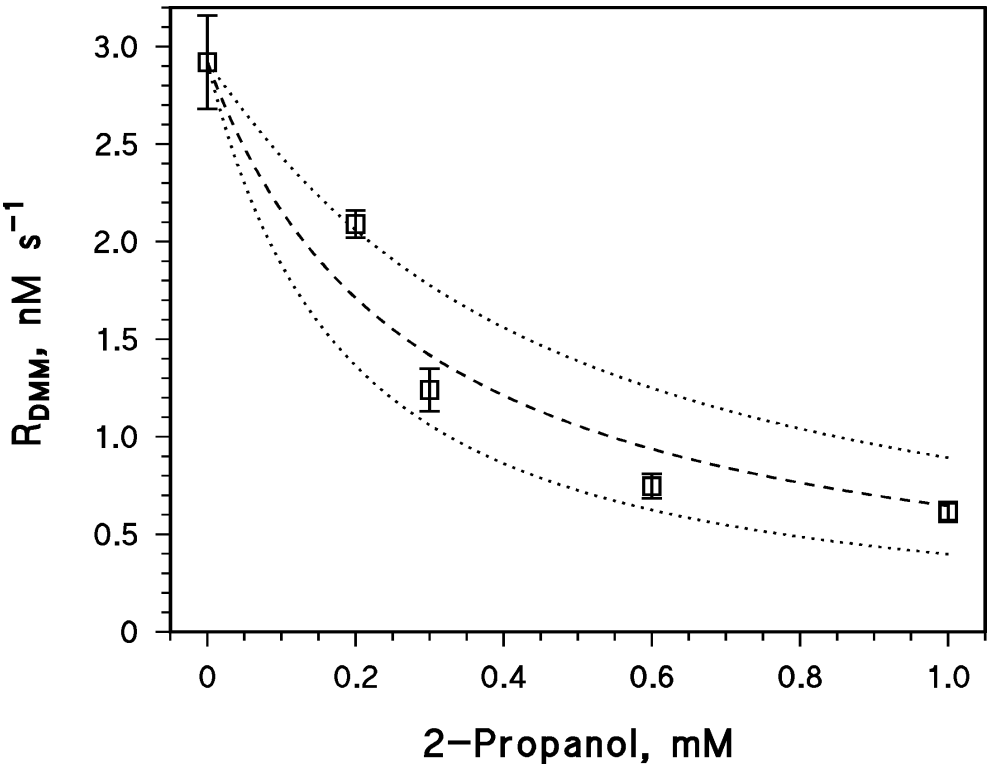

Figure 2. Initial transformation rates of 20 μM DMM upon UVB irradiation of 1 mM H_2O_2, as a function of the concentration of added propan-2-ol at pH 7.

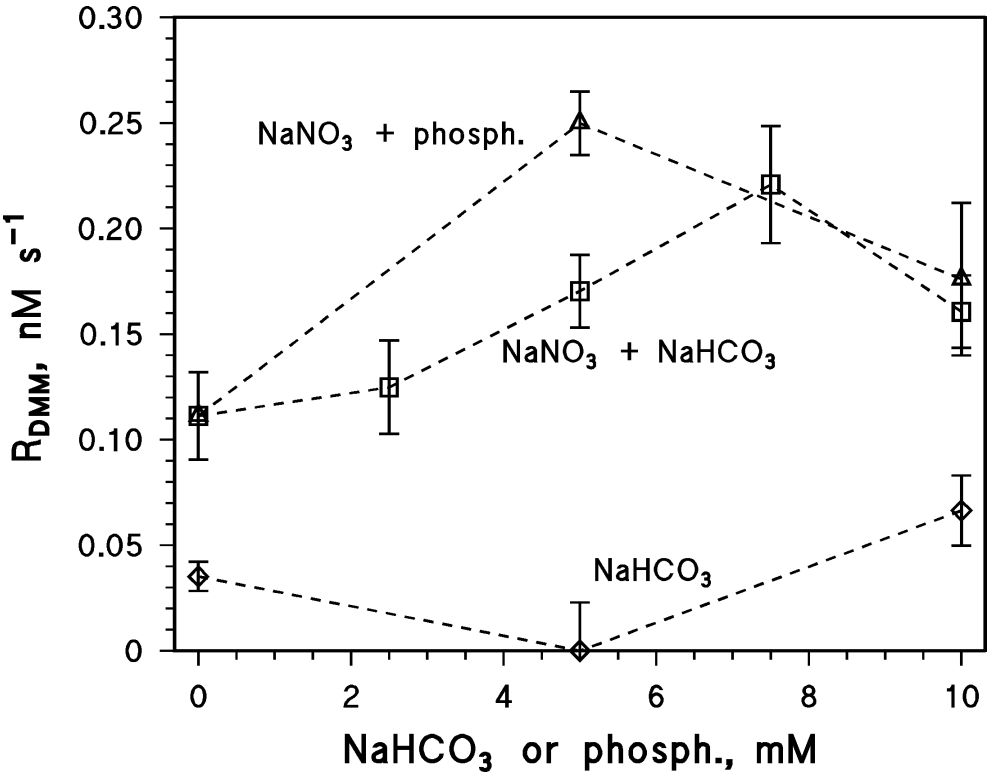

Figure 3. Initial transformation rates under UVB irradiation of (□) 20 μM DMM and 10 mM $NaNO_3$, as a function of the concentration of $NaHCO_3$; (Δ) 20 μM DMM and 10 mM $NaNO_3$, as a function of the concentration of added phosphate buffer (same concentration as $NaHCO_3$ and same pH, within 0.1 units); (◊) 20 μM DMM, without nitrate, as a function of $NaHCO_3$ concentration.

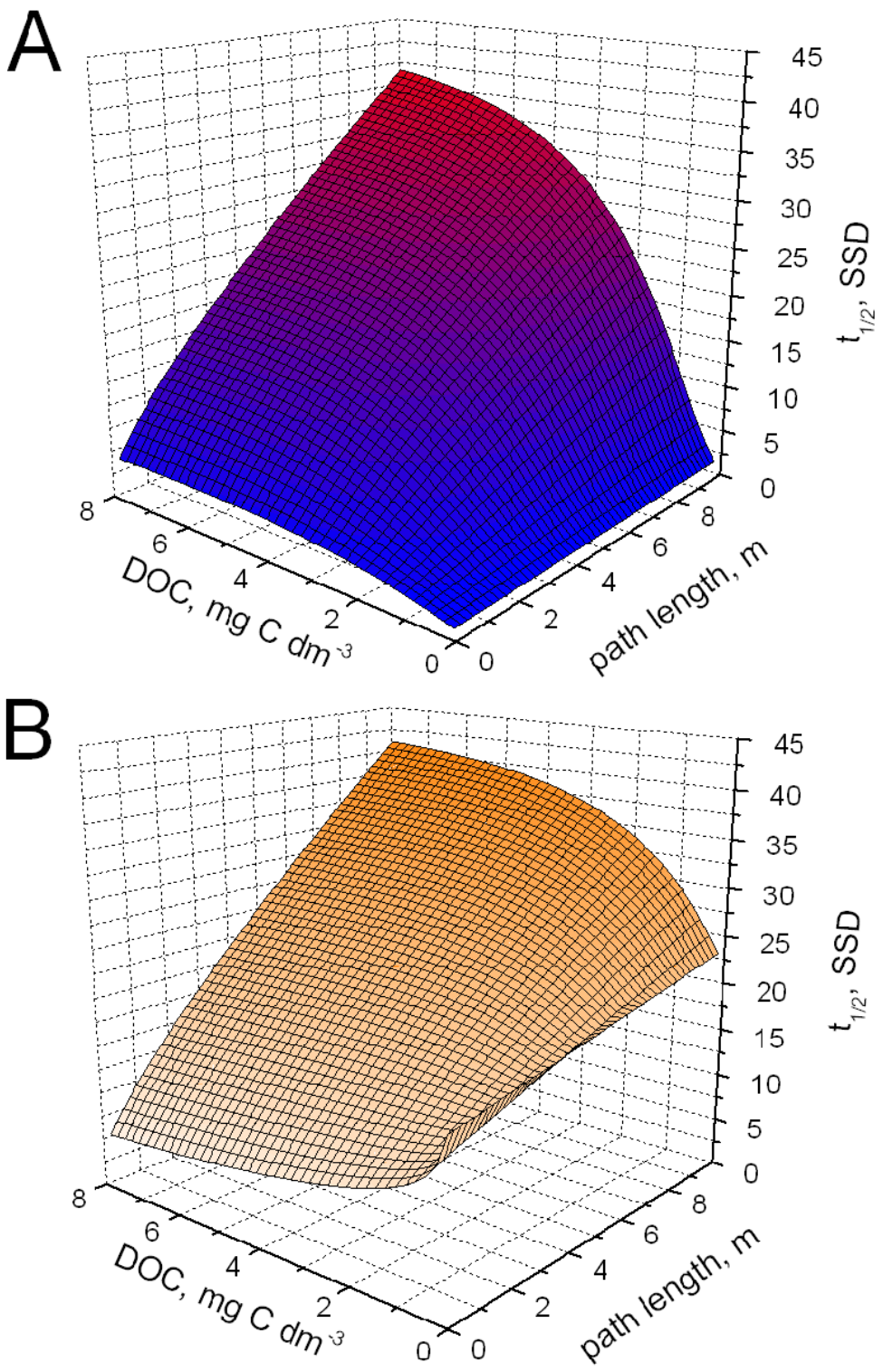

Figure 4. Photochemical half-life time of DMM, as a function of DOC and of the optical path length l of sunlight in water. To compare with the water depth d, note that l = 10 m means d = 8.5 m on 15 July at 45°N latitude. SSD = summer sunny days equivalent to fair-weather 15 July at 45°N latitude. Other water conditions: **(A)** 0.1 mM nitrate, 1 µM nitrite, 1 mM bicarbonate, 10 µM carbonate; **(B)** 1 µM nitrate, 10 nM nitrite, 1 mM bicarbonate, 10 µM carbonate.

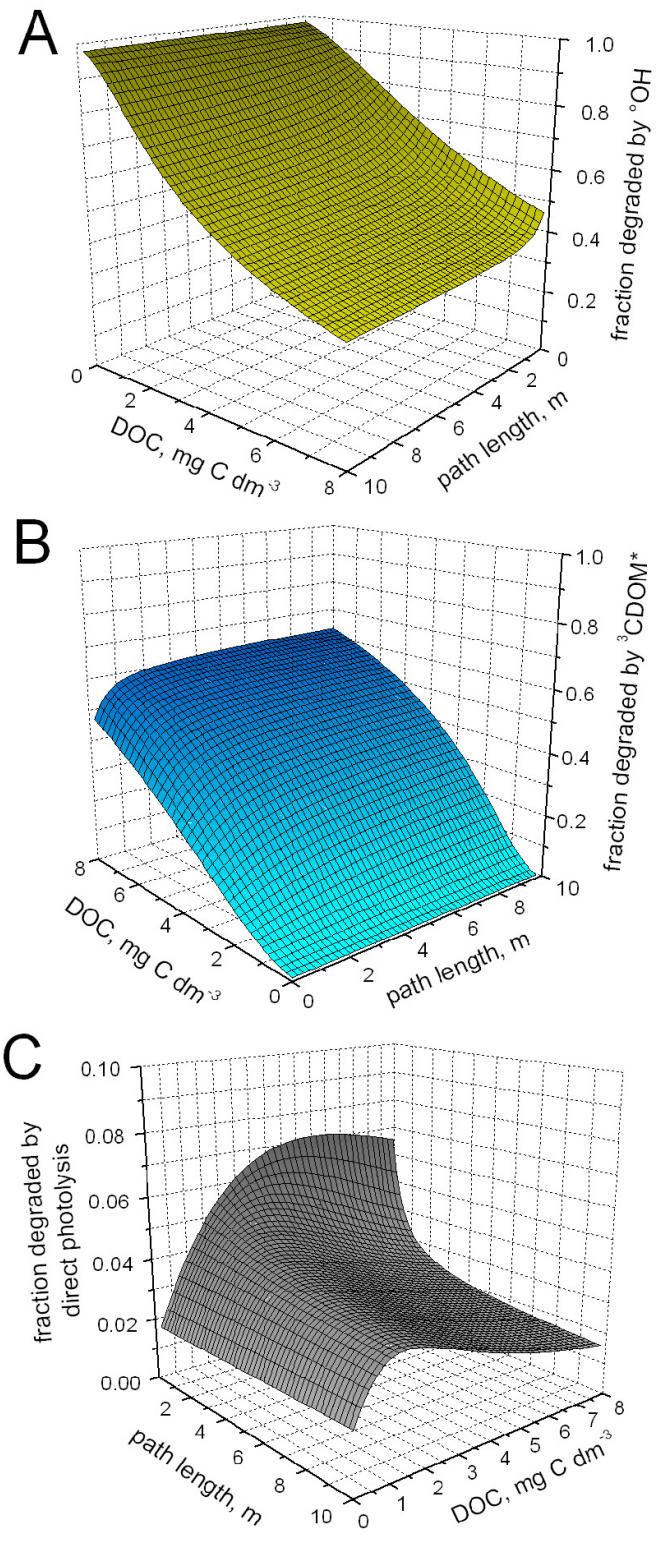

Figure 5. Fractions of DMM photochemical transformation accounted for by **(A)** $^{\bullet}$OH, **(B)** ^{3}CDOM* and **(C)** direct photolysis, as a function of DOC and the optical path length *l*. Other water conditions: 0.1 mM nitrate, 1 µM nitrite, 1 mM bicarbonate, 10 µM carbonate.

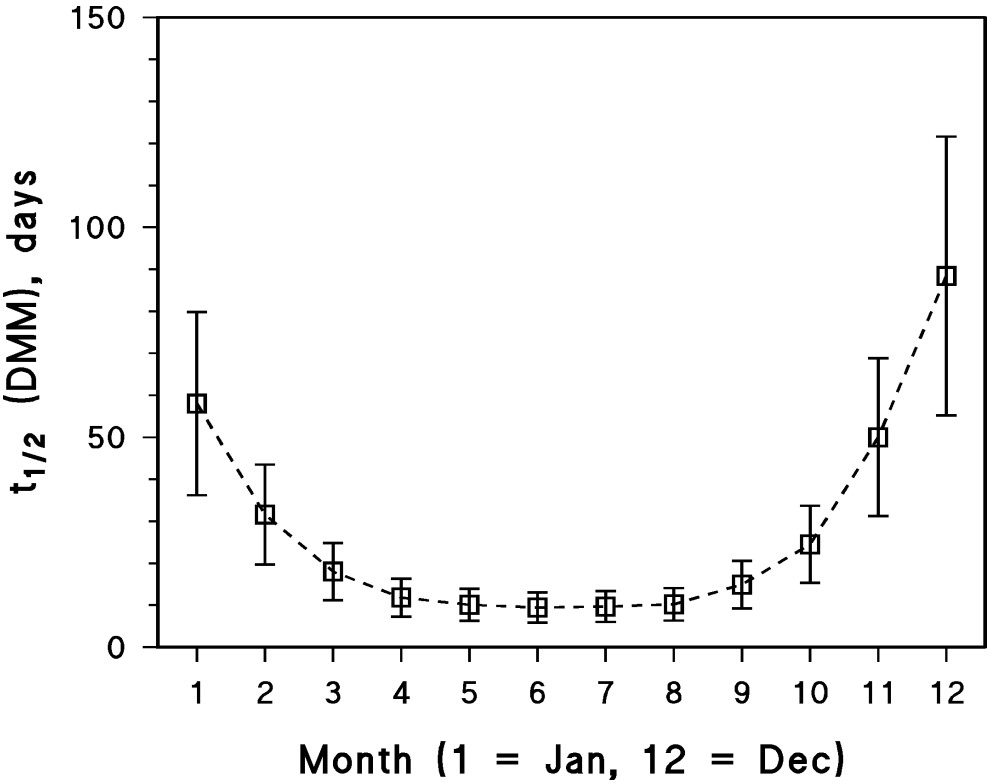

Figure 6. Photochemical half-life time of DMM as a function of the month of the year. The time unit is a fair-weather day corresponding to the 15th of the relevant month. Water conditions: sunlight path length l = 2 m, NPOC = 3 mg C L^{-1}, 0.1 mM nitrate, 1 µM nitrite, 1 mM bicarbonate, 10 µM carbonate.